The 7th International Conference on Discrete Element Methods
August 1 to August 4, 2016 Dalian, China
Paper Number: G010111

Algorithms and Capabilities of *Solidity* to simulate interactions and packing of complex shapes

Jiansheng Xiang[1], John-Paul Latham, Ado Farsi

ABSTRACT: A number of numerical algorithms for simulation of particle packing have been proposed and used in a wide range of industries: mining, chemical engineering, pharmaceuticals, agriculture and food handling, etc. However, most of them can only deal with simple and regular shapes due to the complex and expensive numerical algorithms needed to simulate complex shapes. In this paper, a FEMDEM code, *Solidity*, is used to more accurately capture the influence of complex shape. It combines deformable fracturing arbitrary-shaped particle interactions modelled by FEM with discrete particulate motion modelled by DEM. This paper will cover recent code optimisation for the contact force calculation with arbitrary body shape, parallelisation performance and discussion of results showing both deformable and rigid body versions of the code in different application scenarios. *Solidity* also provides post-processing tools to analyse the particle packing structure in terms of local porosity and orientation distributions, contact forces, and coordination number, etc. Some examples of Platonic and Archimedean body packs are presented.

Keywords: FEMDEM, complex-shaped bodies, packing simulations.

1. Introduction

Particle packing has been studied for many years as it is of fundamental importance to many industries: mining, chemical engineering, pharmaceuticals, agriculture and food handling, etc. In previous years, most published papers have been on packing of spherical particles using the Distinct or Discrete Element

[1] J. Xiang (✉)
Applied Modelling and Computation Group,
Department of Earth Science and Engineering,
Imperial College London,
South Kensington Campus, London SW7 2AZ, United Kingdom
e-mail: j.xiang@imperial.ac.uk

Method (DEM) which was invented by Cundall and Strack (Cundall and Strack, 1979).
Recently, the packing of complex shapes has been attracting more and more interest motivated by their wide application in industry. A number of numerical algorithms for simulation of particle packing have been proposed. Greben et al, (2010) use a commercial code popular in the video games industry, PhysX (by Navidia) to place packs of armour units such as Antifer Cubes and Dolosse. Blender, is a similar module with certain physically realistic features used to introduce mechanical realism into computer animation visualisations. DigiPack (Caulkin et al. 2008) was used to simulate the structure pattern of catalyst pellets. Some researchers also developed so-called clustered overlapping sphere algorithms to represent non-spherical shapes and simulate them in DEM. Cleary (2008) used the so-called superquadrics and formulas to define ellipsoids or other quadrics. However, most of them can only deal with simple and regular shapes due to the complex and expensive numerical algorithms needed to simulate complex shapes.
The Finite Element Method, (FEM), for modelling stress and deformation of solids, has for several decades now, been combined with DEM for modelling the collision and motion of solids. Important for handling complex shapes, FEMDEM solves the contact mechanics using a distributed contact force approach. In this paper, a FEMDEM code, *Solidity*, is used to more accurately capture the influence of complex shape. This paper will cover recent code optimisation for the contact force calculation with arbitrary body shape, parallelisation performance and discussion of results showing both deformable and rigid body versions of the code in different application scenarios. *Solidity* also provides post-processing tools to analyse the particle packing structure in terms of local porosity and orientation distributions, contact forces, and coordination number, etc.
The paper is organised as follows: Section 2 briefly describes the mathematical models, in Section 3 applications and some results are shown followed by a conclusion.

2. Mathematical models

The FEMDEM method was pioneered by Munjiza whose first working 2D FEMDEM code was developed in 1990 (Munjiza 2004). FEMDEM has proven its efficiency and reliability as a computational tool to solve problems involving transient dynamics of systems in which deformation and fracturing play an important role. Xiang et al. (2009) introduced higher order large strain improvements in their FEMDEM code, named Y3D-D. Y3D-D handles the transient dynamics of complex shaped multi-body behaviour and can support a vast range of alternative e.g. non-linear constitutive or internally fracturing properties. Recently, the first author (Xiang) has developed a new version of the original Y3D to simulate rigid solids. This rigid body solver, has the advantage that it executes the simulation faster than the general deformable version.

2.1 Governing equations

1. Deformable solid

The motions of elements are influenced by the forces acting on elemental nodes, internal nodal force, $\mathbf{f}_{\text{int}}$, external nodal force, $\mathbf{f}_{ext}$. The constitutive equation influences the deformation of the material through the Cauchy stress tensor in the linear momentum equation given by,

$$\mathbf{M}\dot{\mathbf{v}}_n^T + \mathbf{f}_{\text{int}} = \mathbf{f}_{ext} + \mathbf{f}_c \tag{1}$$

Where **v** is nodal velocity vector, Internal nodal forces are given by

$$\mathbf{f}_{\text{int}} = \int_{v^{(n)}} \frac{\partial \mathbf{N}}{\partial \mathbf{x}} \mathbf{T} dv \tag{2}$$

External nodal forces are given by

$$\mathbf{f}_{ext} = \int_{v^{(e)}} \mathbf{N}\mathbf{b} dv + \int_{v^{(e)}} \mathbf{N}\mathbf{t} da \tag{3}$$

Where **b** is body force, defined by $\mathbf{b} = \lfloor b_x \quad b_y \quad b_z \rfloor$, **t** is surface traction force.

Nodal mass matrix is given by,

$$\mathbf{M} = \int_{V_0} \rho_0 \mathbf{N}\mathbf{N}^T dV \tag{4}$$

Since mass is conserved, the mass is calculated based initial configuration. ρ is the density of material.

2. Rigid body solid

$$m_{p,i}\dot{\mathbf{v}}_{p,i} = \mathbf{f}_{d,i} + m_{p,i}\mathbf{g} + \sum_{j=1}^{k_i} \left(\mathbf{f}_{cn,ij} + \mathbf{f}_{ct,ij} \right)$$

(1)

$$I_{p,i}\ddot{\boldsymbol{\theta}}_{p,i} = \sum_{j=1}^{k_i} \mathbf{T}_{c,ij} \tag{2}$$

where $m_{p,i}$ and $I_{p,i}$ are mass and moment of inertia of the particle i, respectively. $\ddot{\mathbf{x}}$ and $\ddot{\boldsymbol{\theta}}$ are the linear acceleration and angular acceleration of the particle *i*, respectively. $\mathbf{T}_{\text{c,ij}}$ is contact force torque. For multiple interactions, the interparticle forces and torques are summed for k_i elements interacting with particle *i*.

2.2 Contact force

In FEM/DEM, a penalty function method is employed to calculate the normal contact force when two particles are in contact. The penalty function method in its classical form assumes that two particles penetrate each other. The elemental contact force is directly related to the overlapping area of finite element in contact. The distributed contact force approach takes into account the shape and the size of the overlap area in order to be distributed among the surrounding nodes. Munjiza [5] showed that integration over finite elements was equivalent to integration over finite element boundaries, the contact force is given by,

$$\boldsymbol{f}_n = \sum_{i=1}^{n}\sum_{j=1}^{m}\int_{\Gamma_{\beta_{c_i}\cap\beta_{t_j}}} \boldsymbol{n}_{\Gamma_{\beta_{c_i}\cap\beta_{t_j}}} \left(\varphi_{c_i} - \varphi_{t_j}\right) d\Gamma \tag{3}$$

Where β_c and β_t are the contactor and target discrete elements, respectively, $\boldsymbol{n}$ is the outward unit normal to the boundary of the overlapping area, the integration over finite element boundaries can be written as summation of integration over the edges of finite elements.

Xiang et al (2009) developed further the FEMDEM method by taking account of the sliding friction force. The well-known classic Coulomb type friction was implemented and described as follows,

$$\boldsymbol{f}_t = -k_t\boldsymbol{\delta}_t - \eta\boldsymbol{v}_t \tag{4}$$

where η is the coefficient of viscous dissipation, $\boldsymbol{f}_t$ is the tangential elastic contact force and $\boldsymbol{v}_t$ is the tangential relative velocity. If $\boldsymbol{f}_t$ is bigger than the friction force obeying the Coulomb-type friction law, $\left|\boldsymbol{f}_t\right| > \mu\left|\boldsymbol{f}_n\right|$ the particles slide over each other and the tangential force is calculated using the total normal contact force $\boldsymbol{f}_n$:

$$\boldsymbol{f}_t = -\mu\boldsymbol{f}_n \tag{5}$$

where μ is the coefficient of sliding friction.

2.3. Code optimisation and parallelisation

High CPU cost hinders FEMDEM methods from being more widely used especially when in-efficient and serial algorithms. Recently Xiang optimized the contact detection algorithm in the FEMDEM and parallelized the code using OpenMP. In this paper, the authors use a packing system with 288 rock-like boulders to test the CPU time resulting from these speed enhancements. Figure 1 shows the FEMDEM capability to model such a system of mono-sized angular rock-like boulders (bodies of about 40 kg) being dumped in a 5.26m×5.3m×3.87m bin (front face not shown). The OpenMP parallelised code is shown (Figure 1) to give a speedup of 6.5 on 8 threads and 9 on 12 threads in a 3D deformable rock deposition with 288 particles. The runtime was reduced by half after the code was optimized. In future, the OpenMP implementation will be redesigned with a hybrid MPI and OpenMP implemented for larger particle systems to be modelled.

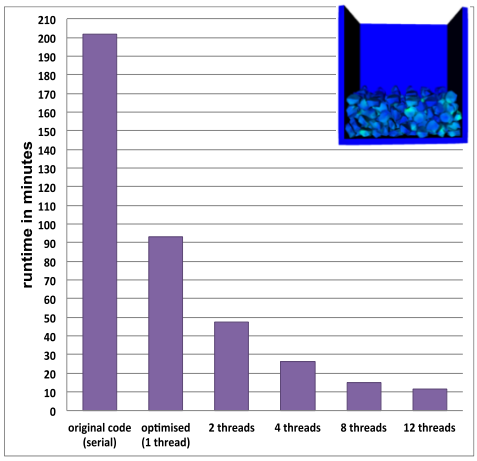

Figure 1 Speed-up achieved by Solidity

3. Results and discussions

3.1 simulation setup

Inspired by the work of Torquato and Jiao (2009), a random packing protocol is used to prepare the packing of 5 Platonic (Figure 2) and 13 Archimedean (Figure 3) solids in a rectangular container. About 11,000 particles are added sequentially at a certain height from the highest position of the existing particles in the container. This ensured that the particles land in a stable configuration without adding variable and excessive impact energy to the particles which were already in place in the packing. In this paper, the particles are modelled as rigid bodies with density of 2.56 g/cm^3 and Coulomb coefficients of friction from 0.2-1.0, together with a damping coefficient of 0.6. Note, that all eighteen particle geometries have been given the same size, d defined by the diameter of the circumscribing sphere, and thus have different volumes.

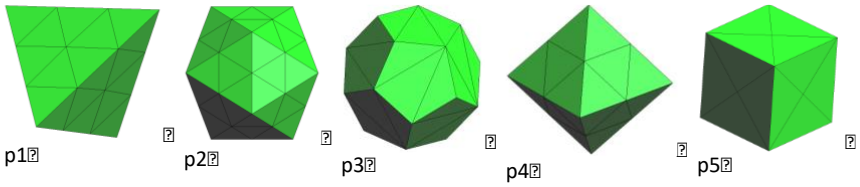

Figure 2. The five Platonic solids: tetrahedron P1, icosahedron P2, dodecahedron P3, octahedron P4, and cube P5.

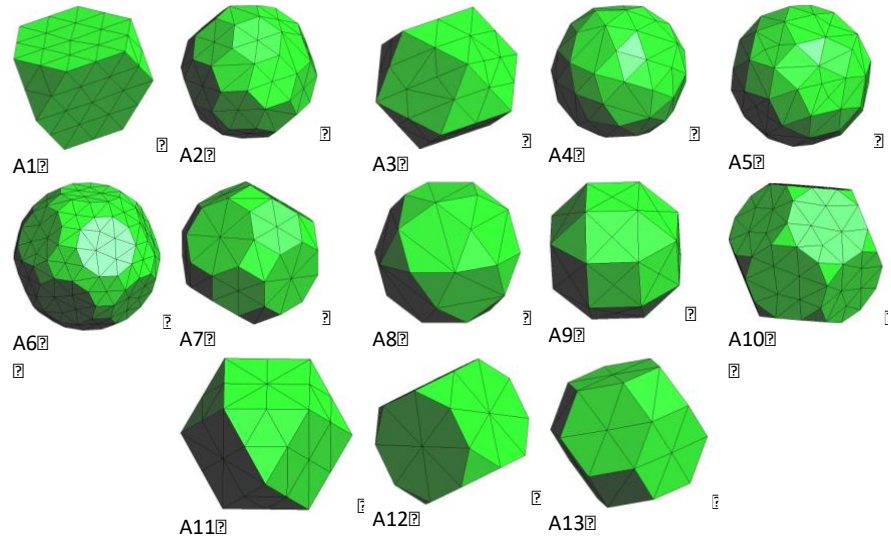

Figure 3. The 13 Archimedean solids: truncated tetrahedron A1, truncated icosahedron A2, snub cube A3, snub dodecahedron A4, rhombicosi dodecahedron A5, truncated icosidodecahedron A6, truncated cuboctahedron A7, icosidodecahedron A8, rhombicub octahedron A9, truncated dodecahedron A10, cuboctahedron A11, truncated cube A12, and truncated octahedron A13.

3.1 Packing Density

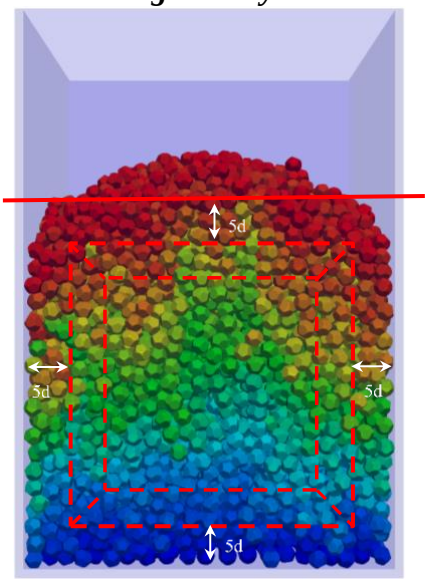

Figure 4 Final simulated packing structure for the truncated dodecahedron dodecahedron (solid shape A10) as seen from the front face container wall, colour indicates sequence of placement.

An example pack is shown in Figure 4, where the bulk packing sample volume for average porosity calculation is described as being bounded by moving in from the container wall by 5d, and for the case of the uneven top, the 5d is taken inwards from the average horizontal plane for the top surface particles. Porosity in a granular system is the volume fraction of voids in a total volume of a granular system, the volume fraction of solids being the packing density. A regular grid is defined in the domain of the numerical results. A value of 1 is assigned to the centroid of the cells that are inside a tetrahedron of the solid mesh and 0 is assigned otherwise. For the sake of clarity in Figure 5 for illustrative purposes, the cell dimension is shown to be similar to the dimension of the cylindrical pellets. This algorithm can be used to calculate mean packing density in this paper or local packing density distribution in (Farsi, et al, 2016).

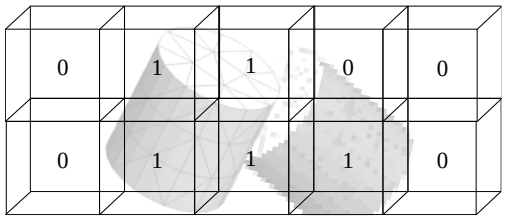

Figure 5 Representation of packing density calculation

Table 1 Packing density

	Packing density
truncated tetrahedron A1	0.57
snub cube A3	0.55
rhombicosi dodecahedron A5	0.57
truncated cuboctahedron A7	0.56
truncated dodecahedron A10	0.54
truncated octahedron A13	0.56
tetrahedron P1	0.52
icosahedron P2,	0.56
dodecahedron P3	0.56
octahedron P4	0.55
cube P5	0.52

Five Platonic (P1-5) and 6 Archimedean (A1, A3, A5, A7, A10, and A13) solids are investigated at this stage. They are deposited in the container using a sequential addition protocol with a friction coefficient 0.6. The mean packing densities are shown in Table 1. Packing densities for all 11 solids vary in a narrow range, 0.52-0.57. a reflection on the low energy from particle impact velocity available for

translation and reorientation with this level of applied Coulomb friction. However, it is interesting to note that the square and the tetrahedron, particles that are clearly having highest angularity and lowest sphericity, have considerably lower packing density. The truncated tetrahedron A1 was selected to illustrate the effect of friction.

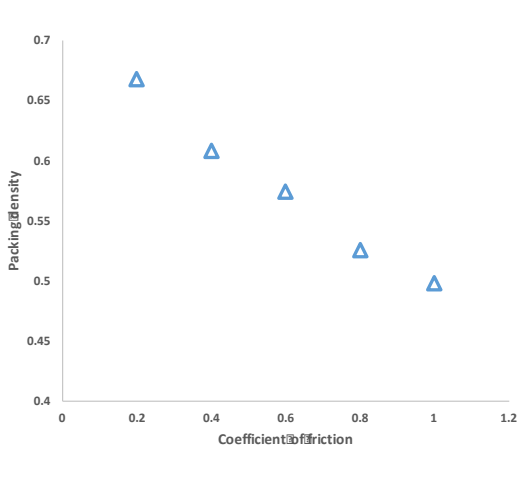

Figure 6 Packing density vs friction coefficient for solid shape A1

The effects of friction coefficient on packing density is shown in Figure 6. As expected, the higher the friction coefficient, the lower packing density for A1 shape. This trend qualitatively agrees with the results found by other researchers (Zhao, et al. 2015). When friction coefficient is reduced to 0.2, the packing density reaches 0.67. This value matches very well with the the density of the optimal lattice. Packing of truncated tetrahedron, 0.68 (Torquato and Jiao, 2009). Further, investigation with these tools can explore extreme dense packing conditions by a combination of low friction and vibration of boundaries.

3.2 Contact forces

The magnitude of contact forces for each unit in the static pack has been extracted. The maximum contact force experienced by each particle is also of interest. Normally the contact force is used to extract the force-chain network and how they change in dynamic systems. In this paper, the force chain network is constructed from a list of all contact forces larger than 1.5 times the mean weight-normalised maximum contact force, i.e. F_c/W for all contacts experienced by all particles.

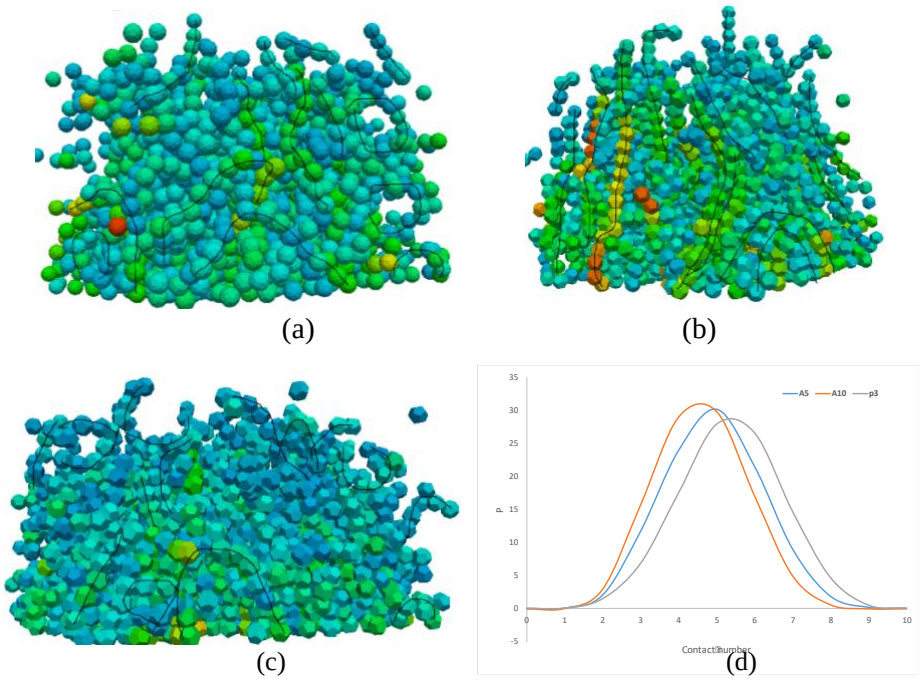

Figure 7 Packing characteristics showing force chains (a, b, c) and coordination number statistics (d): (a) rhombicosi dodecahedron A5, (b) truncated dodecahedron A10, (c) dodecahedron P3, (d) Probability density function, P of normalised contact force.

A class of dodecahedrons, P3, A5 and A10 is selected for analysing the force-chain structure pattern (Figure 7 a-c). It is shown that A10 tends to generate longer and straighter chains which may be due to their bigger facets. P3 and A5 tend to form short and circular networks Arching type structures are found in all three packs near the corners of the container. The three-dimensional force chain structure is easy to illustrate in a changing view 3D visualizer, but is more difficult to display in a figure. In similar work done with 2D FEMDEM simulations (Guises et al 2009), where force-chain and stress-chains were examined using various normalisation strategies, it is much easier to highlight the chain structures and compare with photo-elastic experiments. It should be noted that stress chains can also be analysed, either by running the more CPU-hungry deformable solver, or by importing the rigid pack geometry and re-solving the equilibrium state with the deformable code.

3.3 Coordination number

The number of contacts each particle makes with its neighbours is known as the coordination number. The coordination number has a wide variation; contacts with neighbouring particles or container ranging from 1 to 10 in the three packs examined

for A5 A10 and P3. Different packing conditions result in a different average coordination number and different spatial distributions of coordination number. Fig. 15 shows the variation of coordination number in a probability density plot for the three different packing density packs. From A10 to P3 the probability density curve shifts to the right, resulting in a larger average coordination number and wider spread. It is worth noting that the analysis tools recognise the surface-to-surface and edge-to-surface contacts as one coordination number. Thus, the lowest value of coordination number in these three static packs is one. The analysis tools including force- and stress-chain statistics are continually being improved for the benefit of future granular media analysis.

3.2 Orientation of unit axes

A useful method to examine whether particle principle axes are entering the packing domain with preferred orientation or later adopt one is to use stereographic projection methods. Farsi et al., 2016 (this conference) use *Solidity* to simulate particle structure of cylindrical packs and show the orientation distributions with stereographic analysis.

4. Conclusions

In this paper, we have presented a FEMDEM model that has been developed and parallelised to investigate the random packing of complex shapes. Platonic and Archimedean body packs were investigated and analysed in terms of local porosity and orientation distributions, contact forces, and coordination number, etc. The effect of friction was investigated for truncated dodecahedron particles. Packing density decreases as friction coefficient increases. The sequential addition method of introducing the particles to the already packed grains was set up to give only low levels of energy and with the one friction value tested in this work, relatively low values of packing density will have been created compared with maximum jammed packs that would be possible with different coalescence history and friction parameter selection. The packing density analysis picked out the slightly lower packing densities to be expected for the most angular particle shapes which were the tetrahedrons and cubes.

Acknowledgements

The third author’s research is supported by EPSRC and Johnson Matthey which is gratefully acknowledged.

References

1. Cundall, P.A. and O.D.L. Strack, (1979) Discrete numerical model for granular assemblies. Geotechnique, 29(1): p. 47-65.
2. Munjiza, A., (2004) The Combined Finite-Discrete Element Method, John Wiley & Sons.

3. Williams, J.R. and A.P. Pentland, (1992) Superquadrics and modal dynamics for discrete elements in interactive design. Engineering Computations, 9(2): p. 115-127.
4. Xiang, J., Munjiza, A., Latham, J.-P., and Guises, R. , (2008) On the validation of DEM and FEM/DEM models in 2D and 3D. Engineering Computations, Vol. 26 No. 6, pp. 673-687.
5. Xiang, J., Munjiza, A. and Latham, J.-P., (2009) Finite strain, finite rotation quadratic tetrahedron element for the combined finite-discrete element method. International Journal for Numerical Methods in Engineering, Volume 79 Issue 8, pages 946-978.
6. Caulkin, R., Jia X., Xu C. (2008) Simulations of structures in packed columns and validation by X-ray tomography. Ind Eng Chem Res.
7. Cleary, P.W., Stokes, N., and Hurley, J., (1997) Efficient collision detection for three dimensional super-ellipsoid particles; Proceedings of 8th International Computational Techniques and Applications Conference CTA C97, Adelaide.
8. Baker, J. and Kudrolli, A., (2010) Maximum and minimum stable random packings of Platonic solids, Physical review E 82
9. Zhao, S., Zhou, X., Liu, W., Lai, C., (2015) Random packing of tetrahedral particles using the polyhedral discrete element method, Particuology, Volume 23, Pages 109–117
10. Torquato, S. and Jiao, Y. (2009) Dense packings of the Platonic and Archimedean solids. Nature. 460 (7257), 876-U109.
11. Farsi, J. Xiang, J. P. Latham, M. Carlsson, E. H. Stitt, M. Marigo, (2016) Simulation and characterisation of packed columns for cylindrical catalyst supports and other complex-shaped bodies, The 7th International Conference on Discrete Element Methods, August, Dalian, China.
12. Guises R., Xiang J., Munjiza A., Latham J.-P., (2009) Granular packing: Numerical Simulation and Characterization of the Effect of Particle Shape, Granular Matter. Volume 11 (5):281-292.